First observation of a rotational band and the role of the proton intruder orbital $\pi 1/2^+[431]$ in very neutron-rich odd-odd ^{106}Nb

Y. X. Luo,[1,2] J. O. Rasmussen,[2,3] J. H. Hamilton,[1] A. V. Ramayya,[1] E. Wang,[1] Y. X. Liu,[4] C. F. Jiao,[5] W. Y. Liang,[5] F. R. Xu,[5] Y. Sun,[6,7] S. Frauendorf,[8,9] J. K. Hwang,[1] S. H. Liu,[1,10] S. J. Zhu,[1,11] N. T. Brewer,[1,12] I. Y. Lee,[2] G. M. Ter-Akopian,[13] Yu. Oganessian,[13] R. Donangelo,[14] and W. C. Ma[15]

[1]*Department of Physics, Vanderbilt University, Nashville, Tennessee 37235, USA*
[2]*Lawrence Berkeley National Laboratory, Berkeley, California 94720, USA*
[3]*Department of Chemistry, University of California Berkeley, Berkeley, California 94720, USA*
[4]*School of Science, Huzhou Teachers College, Huzhou 31300, China*
[5]*School of Physics, Peking University, Beijing 100871, China*
[6]*Department of Physics and Astronomy, Shanghai Jiao Tong University, Shanghai 200240, China*
[7]*Institute of Modern Physics, Chinese Academy of Sciences, Lanzhou 730000, China*
[8]*Department of Physics, University of Notre Dame, Notre Dame, Indiana 46556, USA*
[9]*Institut für Strahlenphysik, FZD-Rossendorf, Postfach 510119, D-01314 Dresden, Germany*
[10]*Department of Chemistry, University of Kentucky, Lexington, Kentucky 40505, USA*
[11]*Department of Physics, Tsinghua University, Beijing 100084, China*
[12]*Physics Devision, Oak Ridge National Laboratory, Oak Ridge, Tennessee 37830, USA*
[13]*Flerov Laboratory for Nuclear Reactions, JINR, Dubna, Russia*
[14]*Facultad de Ingenieria, Casilla de Correo 30, 11300 Montevideo, Uruguay*
[15]*Mississippi State University, P. O. Drawer 5167, Mississippi State, Mississippi 39762, USA*

(Received 26 November 2013; revised manuscript received 27 January 2014; published 30 April 2014)

A rotational band was observed for the first time in ^{106}Nb by means of γ-γ-γ and γ-γ-γ-γ measurements of prompt fission γ rays from ^{252}Cf by using the Gammasphere multidetector array. Projected shell model and potential-energy surface calculations were performed and were compared to the experimental data of ^{106}Nb and the previously reported ^{104}Nb. Configurations and spin-parity were assigned to the ground level, low-lying levels, and rotational bandheads of the two Nb isotopes. The new rotational band in ^{106}Nb was interpreted as a $K^\pi = 2^-$ band with a configuration $\pi 1/2^+[431] \times \nu 5/2^-[532]$. The same spin-parity and configuration were assigned to the analogous band in ^{104}Nb. $\pi 1/2^+[431] \times \nu 5/2^+[413]$, $K^\pi = 3^+$ were assigned to the 0.66-μs isomer and explained the $M2$ isomeric decay to the ground in ^{106}Nb. The proton intruder orbital $\pi 1/2^+[431]$ plays an important role in shape evolution with regard to triaxial deformation in these neutron-rich Nb isotopes.

DOI: 10.1103/PhysRevC.89.044326 PACS number(s): 21.10.Re, 23.20.Lv, 27.60.+j, 25.85.Ca

I. INTRODUCTION

Studies of shape transitions, shape coexistence, superdeformation, identical bands, and triaxiality in the $A \sim 100$ neutron-rich nuclear region have long been of interest [1,2]. Neutron-rich Nb ($Z = 41$) isotopes were found to be transitional with regard to triaxial deformation with axially symmetric shapes identified in Y ($Z = 39$) and near maximal triaxiality in Tc ($Z = 43$) and Rh ($Z = 45$) [3–5]. With changing neutron numbers, abrupt shape transitions from near-spherical deformations in $N \leqslant 59$ to large quadrupole deformations in $N \geqslant 60$ were found in neutron-rich Sr ($Z = 38$), Y ($Z = 39$), and Zr ($Z = 40$) isotopes, and a gradual transition at the same neutron numbers in Mo ($Z = 42$) was found.

Lying between these two regions, the studies of Nb (odd-Z, $Z = 41$) isotopes, especially the odd-odd Nb isotopes, are of significance. Strongly deformed collective bands have been established in ^{101,102,103,104,105}Nb [6–9]. With the identification of the $K^\pi = 1^+$ ground-state band in the odd-odd ^{100}Nb [10], sudden shape transitions from spherical to large deformations in the Nb isotopic chain were found to take place at $N = 59$ in contrast to $N = 60$ for Sr ($Z = 38$), Y ($Z = 39$), Zr ($Z = 40$), and Mo ($Z = 42$) isotopes. It is of interest to explore heavier Nb isotopes with greater neutron excess along the isotopic chain. A $T_{1/2}$ of 1.02 s for the ground level of ^{106}Nb was reported in an early paper [11]. In a recent paper [12], a $T_{1/2}$ of 1.01 s and β-delayed neutron-emission probability P_n of ^{106}Nb and other nuclei with $A \leqslant 110$ were measured by fragmentation of a 120-MeV/nucleon ^{136}Xe beam on a Be target at the National Superconducting Cyclotron coupled cyclotrons. An isomer of 890 ± 50 ns at 204.6 keV and another of 800 ± 50 ns at 201.8 keV were found by Genevey *et al.* in an early paper [13], and in a recent paper [14], a half-life of 0.66 μs was remeasured at 204.9 keV by Kameda *et al.* for ^{106}Nb. In the latter paper, microsecond isomers among fission products from in-flight fission of 345 MeV/nucleon ^{238}U were searched at Rikagaku Kenkyusho, and three low-lying levels were reported in ^{106}Nb. However, no information for higher spin levels in the nucleus has been reported.

This paper reports the first identification of a rotational band in ^{106}Nb and the extension of the previously reported band in ^{104}Nb [8]. Projected shell model (PSM) and potential-energy surface (PES) calculations were performed to compare with the experimental data for ^{106}Nb and ^{104}Nb. Discussions will be given below for the configurations, spin-parity assignments,

nuclear structure, and shapes of the nuclei. The important role played by the proton intruder orbital $\pi 1/2^+[431]$ will be discussed.

II. EXPERIMENT AND DATA ANALYSIS

The detection of spontaneous or induced fission γ rays with multi-γ-detector arrays have been proved to be a powerful method and a "gold mine" for the populations and studies of low-to-high spin levels of neutron-rich nuclei [15]. Our experiment was carried out in the Lawrence Berkeley National Laboratory. Prompt γ rays emitted in the spontaneous fission of a 62 μCi ^{252}Cf source were detected by the Gammasphere with 102 Compton-suppressed Ge detectors. Success in exploring very weakly populated regions has been achieved with long runs for data accumulation (in our case, 2 weeks) and the use of less-compressed data cubes. Over 5.7×10^{11} triple- and higherfold coincidence events were collected, factors of 10–100 higher than earlier measurements. A less-compressed cube with one-third less compression [16] was created and was used in the data analysis. Recently, the data were sorted into 1.9×10^{11} fourfold and higherfold coincidence events, and the triple-gated four-dimensional (4D) hypercube data were analyzed and were proved to be very powerful. Some details for data analysis can be found in our previous publications (e.g., Ref. [8]).

Coincidence data were analyzed with the RADWARE software package [16]. The first identification of the transitions in ^{106}Nb was based on cross-checking the coincidence relationship with the other transitions in the nucleus, which includes the previously reported low-lying ones [13,14], and with those of its complementary fission partners ^{142,143,144}La by using both triple- (double-gated) and quadruple- (triple-gated) coincidence data. A high-spin level scheme of the 4*n* fission partner ^{142}La also was found for the first time and will be published in a forthcoming paper [17]. The assignments of transitions to ^{106}Nb also were confirmed by the measurements of the fission-yield ratios between ^{106}Nb and ^{104}Nb in double-gated spectra by changing gates among their different fission partners by comparing the intensity ratios obtained from fission production data [18] (see details below).

Figure 1 depicts an example of the many cross-checking double-gated and triple-gated coincidence spectra used for data analysis of ^{106}Nb. Figure 2 presents an example of the many triple-gated fourfold coincidence spectra for data analysis of ^{106}Nb. In Fig. 1, one sees the transitions identified in ^{106}Nb coincident with the gates that are the 204.8- and 132.8-keV transitions and with the transitions of its fission partners ^{142,143,145}La. Figure 2 is similar but with triple gates at 204.8, 132.8, and 156.7 keV based on the 4D hypercube data. The coincidence relationships shown in Figs. 1 and 2 and in all the cross-checking spectra, especially in several triple-gated fourfold spectra that use the powerful 4D hypercube, provide strong evidence for the assignments of the transitions to ^{106}Nb. Transition energies and relative intensities shown in Table I for ^{106}Nb were measured by using RADWARE's gf3 least-squares peak-fitting routing [16], and the intensities were corrected for detection efficiencies. The energies have uncertainties of

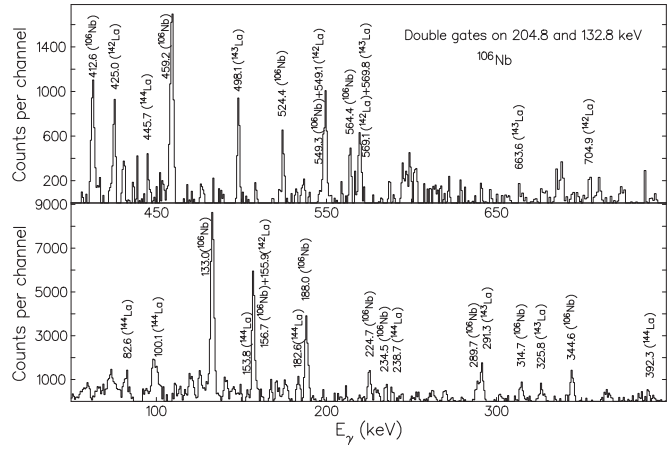

FIG. 1. An example of double-gated triple-coincidence spectra for the data analysis of ^{106}Nb. All the transitions are seen to be in coincidence with the 204.8- and 132.8-keV gates and with the strong transitions of their fission partners.

0.1–0.3 keV, and the intensities have uncertainties from 3% to 10%.

Based on the coincidence relationships, relative intensities of the transitions, and level systematics in the Nb isotopic chain, a level scheme of ^{106}Nb was established as shown in Fig. 3. The spin-parity and configuration assignments for the levels of ^{106}Nb based on PES and PSM calculations are discussed in the following Discussion section. The rotational band observed in ^{106}Nb in the present paper is connected to the ground level via the 204.8-keV isomer in contrast to the observations of a similar rotational band in ^{104}Nb [8] where no linking to the ground was found. However, cross-checking by using the 4D hypercube data resulted in the observation of a weak 130.5-keV transition that decayed from the previously reported bandhead of the band observed in ^{104}Nb [8]. The new level scheme of ^{104}Nb is shown in Fig. 4. The spin-parity reassignments for the levels of ^{104}Nb based on PES and PSM

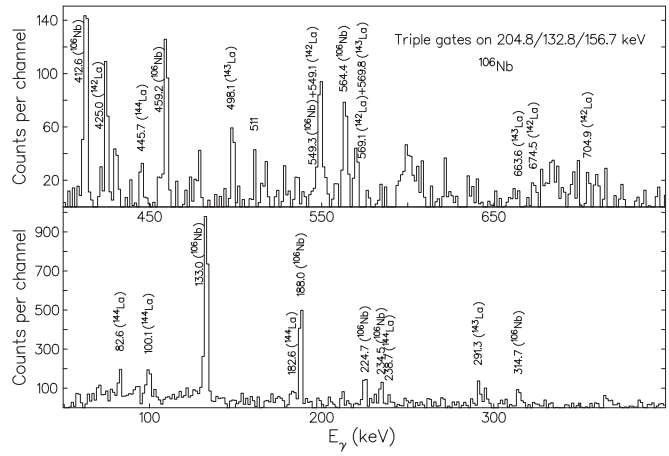

FIG. 2. An example of triple-gated quadruple-coincidence spectra based on the 4D hypercube data for the data analysis of ^{106}Nb. In this spectrum, the gates were set at 204.8, 132.8, and 156.7 keV, strongly supporting the identification of the level scheme of ^{106}Nb. Note how much cleaner the background is now.

TABLE I. Transition energies and relative intensities of the transitions of ^{106}Nb determined in the present paper. Energies with asterisks are the transitions and levels reported in Refs. [13,14] but not observed in the present paper.

^{106}Nb levels (keV)	Spin-parity	Decaying transition energies (keV) and their relative intensities (in brackets)	Band
108.1*	(1^+)	108.1*	
202.2	(2^+)	202.2 (95.4), 94.5*	
204.8	(3^+)	204.8 (100)	
337.6	(2^-)	132.8 (74.2)	1
470.6	(2^-)	133.0 (59.8)	1
627.3	(3^-)	156.7 (30.8), 289.7 (6.5)	1
815.3	(4^-)	188.0 (19.4), 344.6 (14.7)	1
1040.0	(5^-)	224.7 (12.8), 412.6 (10.5)	1
1274.5	(6^-)	459.2 (12.6), 234.5 (4.8)	1
1589.3	(7^-)	549.3 (5.3), 314.7 (2.3)	1
1838.9	(8^-)	564.4 (5.4), 249.7	1
995.0		524.4 (7.5)	2

calculations also are discussed in the following Discussion section.

Ratios of the intensity of the 188.0-keV transition of ^{106}Nb (see Fig. 3) to that of the 185.5-keV transition of ^{104}Nb (see Fig. 4) were measured in gated spectra with gates set at 425.0/569.1, 291.3/498.1, 392.3/548.8, and 472.9/238.1 keV in ^{142,143,144,145}La (the $4n$, $3n$, $2n$, and $1n$ fission partner of ^{106}Nb), respectively, and these ratios were compared to those of ^{106}Mo to ^{104}Mo in ^{142,143,144,145}Ba gates (the $4n$, $3n$, $2n$, and $1n$ fission partner of ^{106}Mo), respectively, obtained from the fission production data reported in Ref. [18] as shown in Fig. 5. In the figure, the similar trends in variations in the ratios $I(^{106}\text{Nb}/^{104}\text{Nb})$ and $I(^{106}\text{Mo}/^{104}\text{Mo})$ with changing gates set in the $4n$, $3n$, $2n$, and $1n$ fission partners, respectively, provide additional confirmation for the transition assignments to ^{106}Nb.

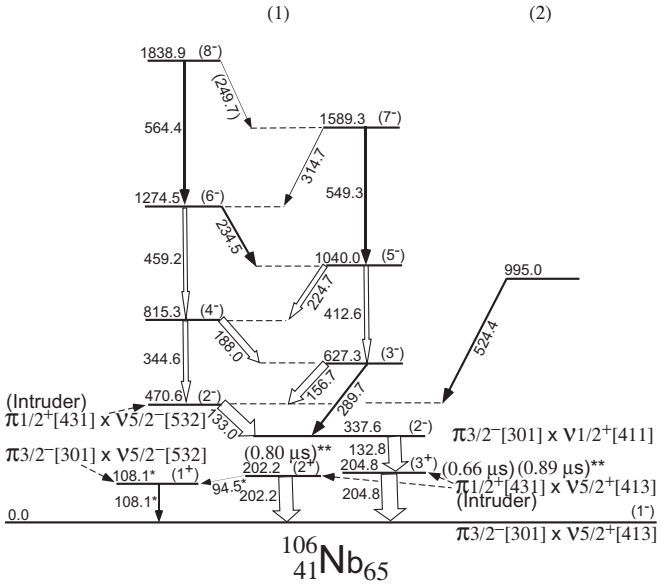

FIG. 3. High-spin level scheme proposed for the first time in ^{106}Nb. A rotational band, band 1, and the 133.0- and 132.8-keV decaying-out transitions were identified in the present paper based on our fission data. Three low-lying levels of 204.8, 202.2, and 108.1 keV were first reported in Refs. [13,14] with no spin-parity assignments, and two of them were confirmed in the present paper. The levels and transitions with asterisks are those reported in Refs. [13,14] but are not identified in the present paper. The half-lives indicated in the figure with double asterisks were given in Ref. [13]. Configurations and spin-parities assigned to the levels in the present paper by PSM and PES calculations are shown in the figure; see the details in the Discussion section.

In Ref. [13], a level scheme of ^{106}Nb with three low-lying levels of 204.6, 201.8, and 107.3 keV and four transitions of 204.6, 201.8, 107.3, and 94.5 keV was established. Two half-lives were reported in Ref. [13] as mentioned in the Introduction (but an averaged half-life of 0.84 μs was shown at the level scheme). In Ref. [14], three low-lying levels at 204.9, 202.1, and 108.1 keV and six transitions of 204.9, 202.1, 108.1, 94.7, 147.5, and 63.5 keV were reported, which confirmed the results in Ref. [13] but gave a half-life of 0.66 μs for the 204.9-keV level. We believe that the 204.8-keV transition assigned to ^{106}Nb in the present paper is the 204.6-keV transition that decays out from the 204.6-keV isomer reported in ^{106}Nb in Ref. [13] and the 204.9-keV transition from the 204.9-keV isomer in Ref. [14]. The $T_{1/2}$ of the isomer reported in Refs. [13,14] did not prevent the observation of the 204.8-keV transition in our experiment since the coincidence time window set in our experiment was $\sim$1 μs. The 201.8-keV transition reported in Ref. [13] (202.1 keV in Ref. [14]) also was identified in our experiment, and it was determined to be 202.2 keV (Fig. 3). In all the gated spectra with gates set in ^{142,143,144}La, one can always see the 202.2-keV transition [17]. However, the parallel 94.5–108.1-keV sequence was not seen in any of these gated spectra, most probably because of the strong background and peak overlaps in the low-energy region based on our fission data with no fission channel selection nor efficient low energy γ and internal conversion electron detections.

We measured the intensity ratios between the 202.2- and the 204.8-keV transitions in the gated spectra with gates set at 425.0/569.1 keV in the $4n$ fission partner ^{142}La and on 291.3/498.1 keV in the $3n$ fission partner ^{143}La, respectively. Ratios of (95.8 $\pm$ 6.6)% and (91.1 $\pm$ 10.5)%, respectively,

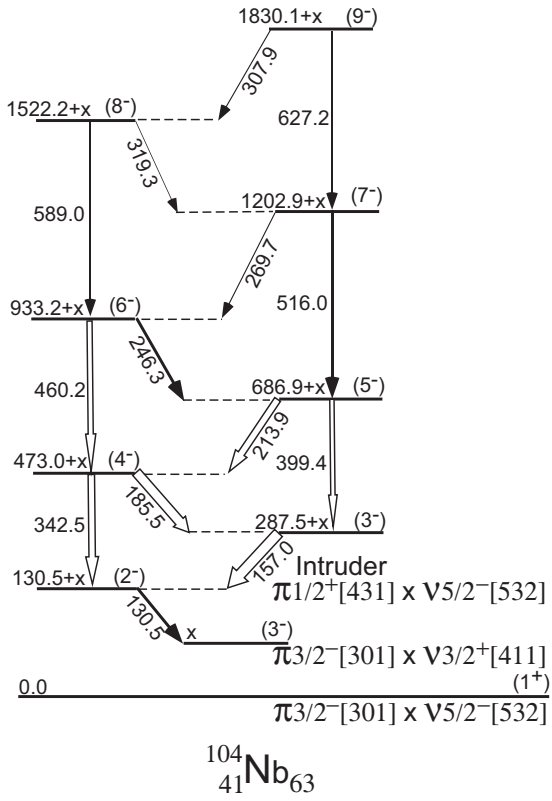

FIG. 4. New high-spin level scheme of ^{104}Nb. By using the triple-gated 4D hypercube data, a weak 130.5-keV transition was identified, which decays from the previously reported bandhead [8]. In Ref. [8], even parity was assigned to the band, and (3^+) was assigned to the bandhead. Configurations and spin-parities reassigned to the levels in the present paper based on the PSM and PES calculations are shown in the figure. See the details in the Discussion section. The missing of the feeding to the ground from the $(130.5 + x)$-keV bandhead and the weak transition of 130.5 keV are most likely due to the unknown half-life of the bandhead, which may be much longer than the coincidence time window set in the experiment. The latter may also be due to there being different proton and neutron orbitals in the initial and final states. The good agreement between experiment and theory for the configuration and spin-parity assignments to the ground and x-keV levels and the PSM-calculated yrast band built on the ground level suggest that, most likely, the 130.5-keV transition does not directly feed the ground. Also, see the discussions in Sec. III C.

were determined in the two gated spectra consistent with each other within the uncertainty range, thus, providing additional evidence that the 202.2-keV transition belongs to ^{106}Nb. Furthermore, in all the gated spectra with gates set at the transitions above the 204.8-keV level in ^{106}Nb, while the strong 204.8-keV transition is seen, the 202.2-keV transition is always missing. In all the gated spectra with one gate set at 202.2 keV and the other set at a transition of a fission partner, no transition was identified to be in coincidence with the 202.2-keV transition by cross-checking. Shown in Fig. 6 is a triple-gated coincidence spectrum with a gate set at 202.2 keV and the other two set at 291.3/498.1 keV of the fission partner ^{143}La. Several strong transitions of ^{143}La are seen in the spectrum, but, by cross-checking the coincidence

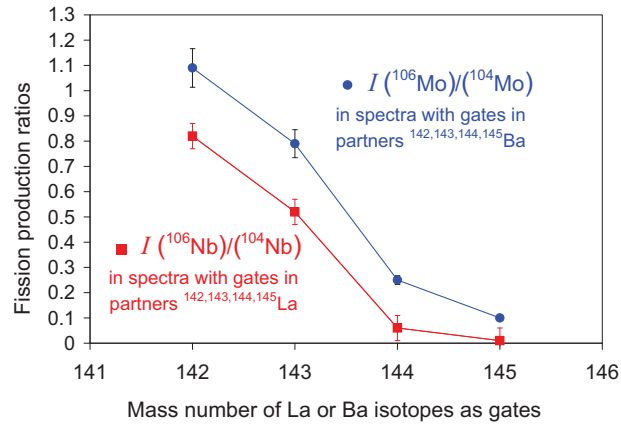

FIG. 5. (Color online) Production ratios $I(^{106}\text{Nb})/I(^{104}\text{Nb})$ plotted with changing gates set in the fission partners ^{142,143,144,145}La. Also shown in the figure are the ratios $I(^{106}\text{Mo})/I(^{104}\text{Mo})$ plotted with changing gates set in the fission partners ^{142,143,144,145}Ba, obtained from the fission data reported in Ref. [18]. The similar trends seen in Nb/La pairs in comparison to Mo/Ba pairs provide additional evidence for the assignments of the transitions to ^{106}Nb. See the text.

relationship, no other transitions, including the ones of ^{106}Nb, were found to be coincident with the triple gates. All the observations mentioned above led to the conclusion that no cascade or transition is built on the 202.2-keV level based on our fission data and there is no linking between the 204.8- and the 202.2-keV levels (see Fig. 3). This conclusion supports

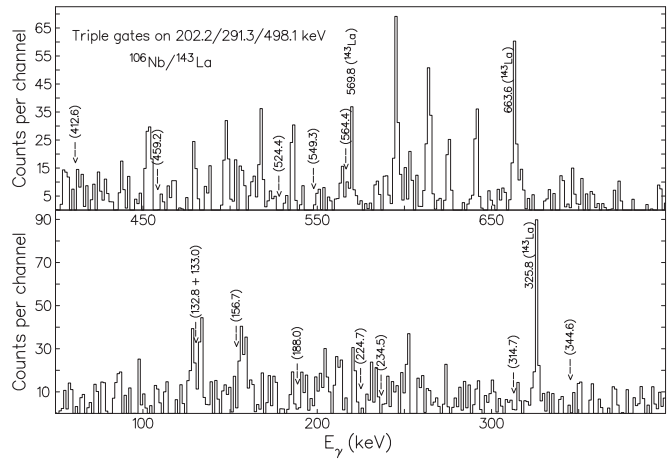

FIG. 6. An example of triple-gated quadruple-coincidence spectra based on the 4D hypercube data for the study of the 202.2-keV level in ^{106}Nb. Gates were set at 202.2 (^{106}Nb) and 291.3/498.1 keV (^{143}La). Arrows and the transition energies in parentheses show the peak positions of the missing transitions of ^{106}Nb. Several strong transitions of ^{143}La are seen in the spectrum, which support the fission partnership of the 202.2-keV transition. Cross-checking the coincidence relationship of the transitions seen in the spectrum has found no other transitions coincident with the triple gates. The missing of coincident transitions with the 202.2-keV one, except for those of the fission partners, implies that the 204.8-keV level does not decay to the 202.2-keV level, and no cascade or transitions are built at the 202.2-keV level.

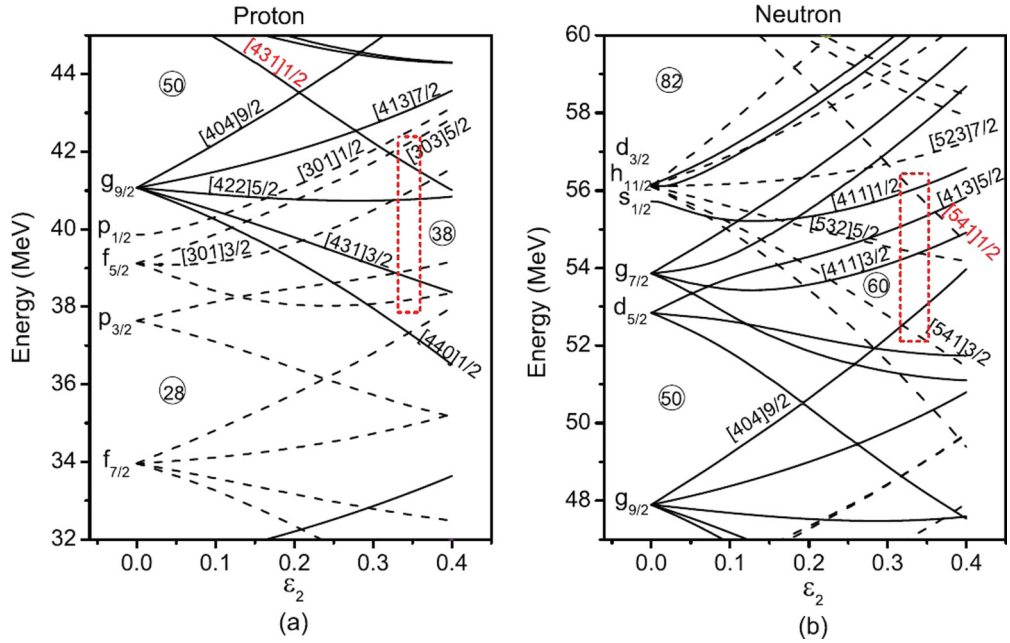

FIG. 7. (Color online) Nilsson diagram that shows the proton and neutron orbitals near the Fermi energy for the Nb fission-fragment isotopes. Note the proton intruder orbital [431]1/2.

the two-half-lives scenario reported in Ref. [13], although the authors showed only an averaged half-life in the level scheme, which can be understood since the measurement conditions were very limited based on the data reported in Ref. [13].

In order to clarify the ambiguity in half-life measurements for the isomer(s) in ^{106}Nb reported in Refs. [13,14], measurements of the half-life of the 204.8-keV level were tried based on our fission data set. With changing timing, variations in the intensity ratio of the 132.8- and 204.8-keV transitions $I(132.8)/I(204.8)$ were determined in a gated spectrum with gates set at the 156.7- and 188.0-keV transitions. Unfortunately, we failed to achieve this goal mainly because the 204.8-, 132.8-, and 133.0-keV transitions of ^{106}Nb have rather large backgrounds in the gated spectra used in the present paper. Since no transition in ^{106}Nb was found in coincidence with the 202.2-keV γ ray, it is not possible to measure the half-life of the 202.2-keV level based on our method by using the data set, and the coincidence relationship between 202.2 keV and those of the fission partners are not sufficient.

Based on the PES and PSM theoretical calculations for ^{104}Nb (see the details in the Discussion section), a different shape with regard to triaxiality in comparison with that of the ground level was suggested for the $(130.5 + x)$-keV level. The $(130.5 + x)$-keV level is most likely an isomer with a half-life considerably longer than the coincidence time window set in the experiment, so no connection to the ground state was observed. Efforts also were made to measure the half-life of the $(130.5 + x)$-keV level in ^{104}Nb. With changing timing, variations in the intensity ratios of the 130.5- and 157.0-keV transitions $I(130.5)/I(157.0)$ were determined with gates set at the 185.5- and 213.9-keV transitions. However, no reliable results could be obtained as is also the case in ^{106}Nb. In view of the good agreement between the theoretical reproduction and the experiment for the x-keV level and ground level and of the PSM- calculated yrast band built on the ground level, most likely, the 130.5-keV transition does not directly feed the ground level (see the details in the Discussion section). Furthermore, based on the spin-parity assignments, the possible ground transition from the x-keV level would be of $M2$ with considerable retardation for the transition. Although no decay-out transitions from the band were identified to feed the ground state in ^{104}Nb, a band pattern very similar to that of ^{106}Nb is seen in ^{104}Nb (Fig. 4).

III. THEORETICAL CALCULATIONS AND DISCUSSION

The ^{104,106}Nb nuclei are in a region where the $g_{9/2}$ proton subshell and the $h_{11/2}$ neutron subshell are beginning to fill. This situation drives prolate spheroidal shapes. However, the $Y_{2,2}$ matrix elements that connect the Nilsson orbitals below with those above the Fermi surface produce a tendency toward triaxiality. This tendency will be stronger in odd-odd nuclei than in their even neighbors because there is no pair breaking involved in forming the triaxial states. However, we will see that the PES calculations below show prolate spheroidal shapes for most odd-odd nucleon orbital choices in ^{104,106}Nb with only a few configurations that show minima that lie between prolate and maximum triaxials, namely, $\gamma \sim 15°$–$9°$. We will also see that an "intruder" proton orbital $1/2^+[431]$ from the $g_{7/2}$ orbitals above the $Z = 50$ shell plays an important role in ^{104,106}Nb.

To address these questions, we have undertaken new theoretical calculations for both isotopes ^{104,106}Nb. PSM calculations [19,20] were performed to determine the excitation energies of the levels, moments of inertia $J^{(1)}$ versus $\hbar\omega$, and $E(I) - E(I-1)$ versus spin and were compared to the experimental data by assuming axially symmetric deformations from Möller *et al.* [21]. To take triaxial deformations into account

TABLE II. Various low-lying excited quasiparticle states calculated by PES for ^{106}Nb. Configurations, shape parameters, excitations, and the spin-parity assigned to the ground level, low-lying levels, and bandhead of the nucleus are indicated in the table. Also, see Fig. 3 and Table IV. It should be emphasized that $\pi 1/2^+[431] \times \nu 5/2^-[532]$ (2^-) were assigned to the bandhead at the 470.6-keV level and the same configuration and spin-parity were assigned to the $(130.5 + x)$-keV bandhead of the analogous band in ^{104}Nb (see Table III). The four configurations with excitations lower than that of $\pi 1/2^+[431] \times \nu 5/2^-[532]$ as listed in the fifth through eighth row, respectively, in the table were definitely excluded by the disagreement between the theoretical calculations and the experimental observations, especially based on the PSM (see Sec. III C).

Configuration	β_2	γ (deg)	β_4	$E_{\rm exc}$ (keV)	Spin-parity assigned
$\pi\frac{3}{2}^-[301] \otimes \nu\frac{5}{2}^+[413]$	0.35	15	0.000	0	(1^-)
$\pi\frac{3}{2}^-[301] \otimes \nu\frac{5}{2}^-[532]$	0.33	14	−0.006	171	(1^+)
$\pi\frac{1}{2}^+[431] \otimes \nu\frac{5}{2}^+[413]$	0.36	2	−0.003	203	$(2^+,3^+)$
$\pi\frac{3}{2}^-[301] \otimes \nu\frac{1}{2}^+[411]$	0.33	0	−0.005	238	(2^-)
$\pi\frac{5}{2}^+[422] \otimes \nu\frac{5}{2}^+[413]$	0.33	17	0.005	319	
$\pi\frac{1}{2}^+[431] \otimes \nu\frac{1}{2}^+[411]$	0.36	2	−0.004	330	
$\pi\frac{5}{2}^+[422] \otimes \nu\frac{5}{2}^-[532]$	0.32	19	0.000	423	
$\pi\frac{5}{2}^-[303] \otimes \nu\frac{5}{2}^+[413]$	0.32	7	0.000	473	
$\pi\frac{1}{2}^+[431] \otimes \nu\frac{5}{2}^-[532]$	0.35	2	−0.005	506	(2^-)
$\pi\frac{5}{2}^+[422] \otimes \nu\frac{1}{2}^+[411]$	0.32	0	0.000	597	
$\pi\frac{5}{2}^-[303] \otimes \nu\frac{5}{2}^-[532]$	0.31	9	−0.003	598	
$\pi\frac{5}{2}^-[303] \otimes \nu\frac{1}{2}^+[411]$	0.32	0	−0.003	619	
$\pi\frac{3}{2}^-[301] \otimes \nu\frac{3}{2}^+[411]$	0.35	8	−0.001	668	
$\pi\frac{1}{2}^+[431] \otimes \nu\frac{3}{2}^+[411]$	0.36	2	0.000	695	
$\pi\frac{1}{2}^+[431] \otimes \nu\frac{1}{2}^-[541]$	0.39	−2	0.013	764	
$\pi\frac{5}{2}^+[422] \otimes \nu\frac{3}{2}^+[411]$	0.35	−7	0.004	986	
$\pi\frac{3}{2}^-[301] \otimes \nu\frac{1}{2}^-[541]$	0.36	9	0.010	1022	
$\pi\frac{5}{2}^-[303] \otimes \nu\frac{3}{2}^+[411]$	0.32	6	0.001	1077	
$\pi\frac{5}{2}^+[422] \otimes \nu\frac{1}{2}^-[541]$	0.35	2	0.017	1360	
$\pi\frac{5}{2}^-[303] \otimes \nu\frac{1}{2}^-[541]$	0.35	−7	0.012	1508	
$\pi\frac{1}{2}^-[301] \otimes \nu\frac{5}{2}^+[413]$	0.32	0	−0.003	1573	
$\pi\frac{1}{2}^-[301] \otimes \nu\frac{1}{2}^+[411]$	0.32	0	−0.004	1645	
$\pi\frac{1}{2}^-[301] \otimes \nu\frac{5}{2}^-[532]$	0.31	0	−0.005	1704	
$\pi\frac{1}{2}^-[301] \otimes \nu\frac{3}{2}^+[411]$	0.33	0	0.000	2121	
$\pi\frac{1}{2}^-[301] \otimes \nu\frac{1}{2}^-[541]$	0.34	1	0.016	2593	

in these Nb isotopes, PES calculations also were performed to provide contour maps of the potential energies for the ground and low-lying states, which included triaxial shapes. We aimed to find interpretations for both ^{104,106}Nb for their ground states, low-lying excited levels, bandheads, and band evolution of the bands observed in ^{104,106}Nb. The explanations for the isomers and bandheads in both isotopes are of great interest.

Figure 7 shows the Nilsson orbitals for a proton and neutron near the Fermi energy in the Nb isotopes. For example, in the PSM calculation, some of the proton and neutron Nilsson orbitals that fall in the rectangles in Fig. 7 are most relevant to the discussions.

A. Model descriptions

In the PSM calculations, the quadrupole and hexadecapole deformations $\varepsilon_2 = 0.342$ and $\varepsilon_4 = 0.053$ suggested in Ref. [21] were adopted and then were slightly adjusted to reproduce the experimental data of ^{106}Nb. A similar treatment was performed for ^{104}Nb. As for the model parameters described in Ref. [19], the monopole-pairing strength is taken to be $G_M = [G_1 \pm G_2(N - Z)A]/A$ for protons and neutrons with $G_1 = 20.25$ and $G_2 = 16.20$ as the coupling constants and "+" for protons and "−" for neutrons. This choice of G_M is appropriate for the single-particle space employed in the PSM where three major shells are used for each type of nucleon ($N = 3$–5 for neutrons and $N = 2$–4 for protons). The quadrupole-pairing strength G_Q is assumed to be proportional to G_M with the proportionality constant fixed at 0.16. These interaction strengths are consistent with those used previously for the same mass region [22].

In the configuration-constrained PES calculations [23,24], the single-particle levels are given by the nonaxially deformed Woods-Saxon potential with the universal parameter [25]. To avoid the possible collapse of pairing in the BCS approach, we use the Lipkin-Nogami (LN) treatment of pairing [26] with

TABLE III. Various low-lying excited quasiparticle states calculated by PES for ^{104}Nb. Configurations, shape parameters, excitations, and the spin-parity assigned to the ground level, low-lying level, and bandhead of the nucleus are indicated in the table. Also, see Fig. 4 and Table IV.

Configuration	β_2	γ (deg)	β_4	$E_{\rm exc}$ (keV)	Spin-parity assigned
$\pi\frac{3}{2}^-[301]\otimes\nu\frac{5}{2}^-[532]$	0.34	9	0.009	0	(1^+)
$\pi\frac{3}{2}^-[301]\otimes\nu\frac{3}{2}^+[411]$	0.34	1	0.013	111	(3^-)
$\pi\frac{1}{2}^+[431]\otimes\nu\frac{5}{2}^-[532]$	0.35	2	0.011	114	(2^-)
$\pi\frac{1}{2}^+[431]\otimes\nu\frac{3}{2}^+[411]$	0.36	2	0.013	170	
$\pi\frac{3}{2}^-[301]\otimes\nu\frac{5}{2}^+[413]$	0.33	13	0.005	197	
$\pi\frac{5}{2}^+[422]\otimes\nu\frac{5}{2}^-[532]$	0.32	14	0.015	300	
$\pi\frac{5}{2}^-[303]\otimes\nu\frac{5}{2}^-[532]$	0.32	7	0.015	421	
$\pi\frac{5}{2}^+[422]\otimes\nu\frac{5}{2}^+[413]$	0.32	16	0.008	425	
$\pi\frac{5}{2}^+[422]\otimes\nu\frac{3}{2}^+[411]$	0.34	0	0.022	425	
$\pi\frac{3}{2}^-[301]\otimes\nu\frac{1}{2}^+[411]$	0.33	0	0.007	545	
$\pi\frac{5}{2}^-[303]\otimes\nu\frac{3}{2}^+[411]$	0.32	6	0.018	583	
$\pi\frac{1}{2}^+[431]\otimes\nu\frac{5}{2}^+[413]$	0.31	10	0.011	599	
$\pi\frac{5}{2}^-[303]\otimes\nu\frac{5}{2}^+[413]$	0.31	10	0.011	599	
$\pi\frac{3}{2}^-[301]\otimes\nu\frac{3}{2}^-[541]$	0.32	15	−0.004	633	
$\pi\frac{1}{2}^+[431]\otimes\nu\frac{1}{2}^+[411]$	0.35	1	0.009	712	
$\pi\frac{5}{2}^+[422]\otimes\nu\frac{3}{2}^-[541]$	0.31	17	0.001	782	
$\pi\frac{5}{2}^+[422]\otimes\nu\frac{1}{2}^+[411]$	0.31	0	0.014	862	
$\pi\frac{5}{2}^-[303]\otimes\nu\frac{1}{2}^+[411]$	0.31	0	0.011	936	
$\pi\frac{5}{2}^-[303]\otimes\nu\frac{3}{2}^-[541]$	0.29	12	0.002	1013	
$\pi\frac{1}{2}^+[431]\otimes\nu\frac{1}{2}^-[541]$	0.39	−2	0.022	1043	
$\pi\frac{1}{2}^+[431]\otimes\nu\frac{3}{2}^-[541]$	0.35	2	0	1175	
$\pi\frac{3}{2}^-[301]\otimes\nu\frac{1}{2}^-[541]$	0.35	0	0.026	1358	
$\pi\frac{1}{2}^-[301]\otimes\nu\frac{5}{2}^-[532]$	0.32	0	0.014	1437	
$\pi\frac{1}{2}^-[301]\otimes\nu\frac{3}{2}^+[411]$	0.33	0	0.018	1558	
$\pi\frac{5}{2}^+[422]\otimes\nu\frac{1}{2}^-[541]$	0.35	0	0.038	1584	
$\pi\frac{1}{2}^-[301]\otimes\nu\frac{5}{2}^+[413]$	0.31	0	0.009	1765	
$\pi\frac{5}{2}^-[303]\otimes\nu\frac{1}{2}^-[541]$	0.34	0	0.033	1870	
$\pi\frac{1}{2}^-[301]\otimes\nu\frac{1}{2}^+[411]$	0.31	0	0.01	1916	
$\pi\frac{1}{2}^-[301]\otimes\nu\frac{3}{2}^-[541]$	0.3	0	0.001	2154	
$\pi\frac{1}{2}^-[301]\otimes\nu\frac{1}{2}^-[541]$	0.34	0	0.032	2807	

pairing strength G determined by the average-gap method [27]. The configuration energy in the LN method can be written as

$$E_{\rm LN} = \sum_{j=1}^{s} e_{k_j} + 2\sum_{k\neq k_j} V_k^2 e_k - \frac{\Delta^2}{G} - G\sum_{k\neq k_j} V_k^4 + G\frac{N-S}{2} - 4\lambda_2 \sum_{k\neq k_j} (U_k V_k)^2,$$

where S is the proton or neutron seniority for the given configuration (i.e., the number of blocked orbits with index k_j) and N is the neutron or proton number. The orbits with index k_j should adiabatically be blocked with varying deformations in the (β_2,γ,β_4) lattice. This has been achieved by calculating and tracking the average Nilsson quantum numbers of orbits involved in the given configuration. The total energy of a state consists of a macroscopic part, which is obtained from the standard liquid-drop model [28], and a microscopic part given by the Strutinsky shell correction [29] $\delta_{\rm shell} = E_{\rm LN} - E_{\rm strut}$. The energy, deformation, and pairing properties of a multiquasiparticle state are determined from the minimum of the configuration-constrained PES. In the model, the excitation energy, which can be compared with experimental data, is defined by the difference between the minima of the multiquasiparticle and the ground-state PESs.

B. Configuration and spin-parity assignments for the ground, low-lying levels, and bandheads in ^{104,106}Nb

Tables II and III show the excitations and shape parameters for various low excited quasiparticle states calculated by PES for ^{106}Nb and ^{104}Nb, respectively, based on various

configurations near the Fermi energy. Spin-parity assigned to the levels also are indicated in the tables. For ^{106}Nb, we assign a configuration $\pi 3/2^-[301] \times \nu 5/2^+[413]$ and spin-parity of (1^-) to the ground level, which has $E_{\rm exc} = 0$ keV, $\gamma = 15°$, $\beta_2 = 0.35$, $\beta_4 = 0.000$ (see Table II). The 108.1-keV level was assigned as (1^+) with a configuration $\pi 3/2^-[301] \times \nu 5/2^-[532]$ in which only a neutron excitation from the ground level is involved. Based on the PES calculations, this configuration has $E_{\rm exc} = 171$ keV (the second lowest) and $\gamma = 14°$, $\beta_2 = 0.33$, $\beta_4 = -0.006$ (Table II), a similar shape to that of the ground level. Then a proton excitation from the ground level is assumed to reproduce the 204.8-keV isomer, with the proton being excited from $\pi 3/2^-[301]$ to the intruder orbital $\pi 1/2^+[431]$ with the neutron orbital unchanged, that is, $\pi 1/2^+[431] \times \nu 5/2^+[413]$, $E_{\rm exc} = 203$ keV, $\gamma = 2°$, $\beta_2 = 0.36$, $\beta_4 = -0.003$, to well reproduce the 204.8- and 202.2-keV levels. With the above configuration assignments, (3^+) and (2^+) were assigned to the 204.8- and 202.2-keV levels, respectively (Table II). The theoretical excitation energy, 203 keV (the third lowest in the calculations), is in good agreement with the experimental values. The occupation of the intruder proton orbital $\pi 1/2^+[431]$ leads to a big shape change in triaxiality parameter γ from 15° in the ground level to nearly a pure prolate spheroid in the 204.8-keV level and retardation for the 204.8-keV $M2$ transition. The 202.2-keV level may also undergo a dramatic change in deformation (from $\gamma = 2°$ to $\gamma = 15°$) due to the intruder driving, which retards the decay of the 202.2-keV level. Based on the configuration assignments, the retardation of the 94.5-keV $M1/E2$ transition out of the 202.2-keV level might also be attributed to different shapes with regard to triaxiality (from $\gamma = 2°$ to $\gamma = 14°$), and there are different proton and neutron orbitals in the initial and final states. The remarkably close half-lives and energies of the 204.8- and 202.2-keV levels in ^{106}Nb can be interpreted by the following arguments: The same configuration was assigned to them, but one adds and the other subtracts proton and neutron projections. In this odd-odd nucleus, the *np* force between unpaired nucleons causes a split, often obeying the Gallagher-Moszkowski rule that the triplet-spin combination of proton and neutron spins be lower in energy than the singlet spin as in the deuteron. However, the proton intruder $1/2^+[431]$ and neutron $5/2^+[413]$ orbitals have different slopes by setting the former (proton) around the polar regions and the latter (neutron) around the equatorial region. Thus, the short-ranged *np* force would only have a small effect.

Going up from the 204.8-keV level, (2^-) is assigned to the 337.6-keV level with a configuration $\pi 3/2^-[301] \times \nu 1/2^+[411]$, which was produced by neutron excitation from the $\nu 5/2^+[413]$ (ground level) to $\nu 1/2^+[411]$ with the proton orbital $\pi 3/2^-[301]$ unchanged. The PES theoretical excitation and shape parameters based on the configuration are $E_{\rm exc} = 238$ keV (the fourth lowest), $\gamma = 0°$, $\beta_2 = 0.33$, $\beta_4 = -0.005$ (Table II). Reasonable agreement with the experimental excitation is achieved, which reveals an axially symmetric shape for the 337.6-keV level. Furthermore, going up from the 337.6-keV level, $\pi 1/2^+[431] \times \nu 5/2^-[532]$, (2^-) are assigned to the 470.6-keV level, the bandhead of band 1 observed in ^{106}Nb, with (3^-) definitely excluded by PSM calculations as discussed below (with regard to the identification of the bandhead, see more arguments given by PSM calculations in the later subsections). The configuration $\pi 1/2^+[431] \times \nu 5/2^-[532]$ is produced by neutron excitation from the $\nu 5/2^+[413]$ (the 204.8-keV level) to $\nu 5/2^-[532]$ with the proton intruder orbital $\pi 1/2^+[431]$ unchanged. The PES theoretical excitation and shape parameters based on the configuration are $E_{\rm exc} = 506$ keV, $\gamma = 2°$, $\beta_2 = 0.35$, $\beta_4 = -0.005$ (Table II). Good agreement with the experimental excitation is achieved, which reveals a nearly axially symmetric shape of the 470.6-keV bandhead and justifies our use of PSM calculations for the energy levels and moments of inertia of the band of ^{106}Nb (see below). As a matter of fact, although the PSM calculations for the odd-odd nucleus could not take the triaxial deformations into account, the calculations suggested the same configuration and spin-parity assignments to the ground state as given by PES calculations (see Table IV). Based on the PSM calculations, the same configuration and spin-parity as given by our PES calculations also were assigned to the 470.6-keV bandhead in ^{106}Nb, although the PSM calculated a higher excitation for the bandhead. In Table IV, we compare our PES and PSM calculations for the ground level and bandhead of ^{106}Nb. The calculations for the other three

TABLE IV. Comparison of the PES and PSM calculations for the ground level, low-lying levels, and bandheads of ^{104,106}Nb. Theoretical excitations $E_{\rm PES}$ by PES and $E_{\rm PSM}$ by PSM (in MeV), configurations, shape parameters, and spin-parity assigned for the levels are indicated in the table. Experimental excitation energies $E_{\rm exp}$ (in MeV) also are shown in the table.

Nucleus	$E_{\rm exp}$	$E_{\rm PES}$	$E_{\rm PSM}$	Spin-parity	Configuration	Shape (PES)	Shape (PSM)
^{106}Nb	0	0	0	(1^-)	$\pi\frac{3}{2}^-[301] \otimes \nu\frac{5}{2}^+[413]$	$\beta_2 = 0.35, \gamma = 15°, \beta_4 = 0.000$	$\beta_2 = 0.417, \beta_4 = 0.079$
	0.1081	0.171		(1^+)	$\pi\frac{3}{2}^-[301] \otimes \nu\frac{5}{2}^-[532]$	$\beta_2 = 0.33, \gamma = 14°, \beta_4 = -0.006$	
	0.2022	0.203		(2^+)	$\pi\frac{1}{2}^+[431] \otimes \nu\frac{5}{2}^+[413]$	$\beta_2 = 0.36, \gamma = 2°, \beta_4 = -0.003$	
	0.2048	0.203		(3^+)	$\pi\frac{1}{2}^+[431] \otimes \nu\frac{5}{2}^+[413]$	$\beta_2 = 0.36, \gamma = 2°, \beta_4 = -0.003$	
	0.3376	0.238		(2^-)	$\pi\frac{3}{2}^-[301] \otimes \nu\frac{1}{2}^+[411]$	$\beta_2 = 0.33, \gamma = 0°, \beta_4 = -0.005$	
	0.4706	0.506	0.660	(2^-)	$\pi\frac{1}{2}^+[431] \otimes \nu\frac{5}{2}^-[532]$	$\beta_2 = 0.35, \gamma = 2°, \beta_4 = -0.005$	$\beta_2 = 0.417, \beta_4 = 0.079$
^{104}Nb	0	0	0	(1^+)	$\pi\frac{3}{2}^-[301] \otimes \nu\frac{5}{2}^-[532]$	$\beta_2 = 0.34, \gamma = 9°, \beta_4 = 0.009$	$\beta_2 = 0.402, \beta_4 = 0.035$
	x	0.111		(3^-)	$\pi\frac{3}{2}^-[301] \otimes \nu\frac{3}{2}^+[411]$	$\beta_2 = 0.34, \gamma = 1°, \beta_4 = 0.013$	
	$0.1305 + x$	0.114	0.444	(2^-)	$\pi\frac{1}{2}^+[431] * \otimes \nu\frac{5}{2}^-[532]$	$\beta_2 = 0.35, \gamma = 2°, \beta_4 = 0.011$	$\beta_2 = 0.402, \beta_4 = 0.035$

levels also are indicated in the table. It should be pointed out that, although good agreement with experiment was achieved for the above-mentioned theoretical calculations, a puzzle remains unexplained about why the 337.6-keV (2^-) level would decay by $E1$ to the 204.8-keV (3^+) level but not by $E1$ to the 202.2-keV (2^+) level in view of the fact that the same configuration was assigned to the latter two levels. Since low-energy $E1$ transitions are always orders of magnitude weaker than Weisskopf single-proton reference lifetimes, the different retardations are not unreasonable. However, further experimental and theoretical work is needed to shed light upon this puzzle. In addition to the studies of configuration and spin-parity assignments to the bandhead in the isotope, we would also like to answer the question of why the feeding is observed predominantly for the more prolate bands with a bandhead at 470.6 keV and for the 204.8- and 202.2-keV levels. Why there are no observed higher-energy members of the latter two states, the microsecond isomeric states, is also a mystery. The feeding preference might be a consequence of the scission process in favoring the more prolate-deformed bands, which match a more stretched prescission shape.

For ^{104}Nb, we assign a configuration $\pi 3/2^-[301] \times \nu 5/2^-[532]$ (1^+) to the ground level, which is calculated to have zero excitations and $\gamma = 9°$, $\beta_2 = 0.34$, $\beta_4 = 0.009$ (see Table III). In comparison to that of the ground level of ^{106}Nb, one can see that only a different neutron orbital is involved, along with a similar β_2 and a slightly smaller triaxial deformation. Whereas, the proton is excited to the intruder orbital $\pi 1/2^+[431]$, a configuration $\pi 1/2^+[431] \times \nu 5/2^-[532]$ is formed in ^{104}Nb, which is the same configuration as that assigned to the bandhead of band 1 in ^{106}Nb as mentioned above. However, most likely because only proton excitation is involved in the case of ^{104}Nb, in contrast to both the proton and the neutron excitations involved to form the same configuration in ^{106}Nb, the configuration $\pi 1/2^+[431] \times \nu 5/2^-[532]$ is calculated to occur at an excitation as low as 114 keV in ^{104}Nb (and $\gamma = 2°$, $\beta_2 = 0.35$, $\beta_4 = 0.011$). Thus, the $\pi 1/2^+[431] \times \nu 5/2^+[413]$, which results in the ($3^+$) for the 204.8-keV isomer of ^{106}Nb, is now bypassed since it is calculated to occur at an excitation as high as 599 keV in ^{104}Nb, most probably because both proton and neutron excitations are involved in ^{104}Nb in contrast to the only proton excitation involved to form the same configuration in ^{106}Nb. The theoretical estimates above may explain the absence of the (3^+) and (2^+) levels in ^{104}Nb. The $\pi 1/2^+[431] \times \nu 5/2^-[532]$ and (2^-) are, thus, assigned to the $(130.5 + x)$-keV level, the bandhead of the band in ^{104}Nb. Assignment of (3^-) to the bandhead is definitely excluded by PSM calculations as discussed in the following subsection. Although the $\pi 1/2^+[431]$ and $\nu 5/2^+[413]$ excitations from the ground level that forms the (3^+) and (2^+) levels were bypassed in ^{104}Nb, the $\nu 3/2^+[411]$ excitation from the ground level is calculated by PES to occur at an excitation as low as 111 keV (the second lowest in excitations in the PES calculations) in the nucleus. $\pi 3/2^-[301] \times \nu 3/2^+[411]$ (3^-) is, thus, assigned to the x-keV level of ^{104}Nb. The PES theoretical shape parameters based on the configuration are $\gamma = 1°$, $\beta_2 = 0.34$, $\beta_4 = 0.013$, a nearly axially symmetric shape. As mentioned in the previous section, the $(130.5 + x)$-keV level, the bandhead of ^{104}Nb, is most probably an isomer with a half-life considerably longer than the coincidence time window set in the experiment. The 130.5-keV transition that decays out of the $(130.5 + x)$-keV level and feeds the x-keV one with very low intensity is most probably due to both the long half-life of the $(130.5 + x)$-keV level in comparison to the experimental time window and the possible retardation caused by there being different proton and neutron orbitals in the initial and final states, although the initial and final states have similar shapes. In view of the above-mentioned spin-parity and configuration assignments for the ground level (1^+), the x-keV level (3^-), and the good agreement between the experiment and the theory, we feel it reasonable to assume that the 130.5-keV transition does not directly feed the ground level. The (1^+) yrast band built on the ground level calculated by PSM shown in the next subsection may provide further support for this assumption. The $M2$ character of the possible transition from the x-keV level that feeds the ground would further retard the transition and would make it unobservable in the experiments to date. As in the case of ^{106}Nb, the PSM and PES calculations resulted in the same configuration and spin-parity assignments to the ground level and bandhead of the rotational band in ^{104}Nb (see Table IV). The PES calculated a nearly axially symmetric shape for the bandhead, which again justifies our use of PSM calculations for the energy levels and moments of inertia of the band of ^{104}Nb (see below).

The above-mentioned interpretations and assignments were made not only based on the agreement between the theory and the experiment with regard to excitation energies and the explanations for the isomers, but also were supported by the following arguments: The same proton orbital $\pi 3/2^-[301]$ is involved in the configuration of the ground level in ^{104}Nb and ^{106}Nb with only different neutron orbitals in the two isotopes. The (1^+) assignment for the ground level of ^{104}Nb is in agreement with that given in the previous studies. The same configuration $\pi 1/2^+[431] \times \nu 5/2^-[532]$ and spin-parity (2^-) were assigned to the bandheads of the analogous bands in ^{106}Nb and ^{104}Nb. The proton excitation and the occupation of the proton intruder orbital $\pi 1/2^+[431]$ causes a change in triaxial deformation and retardation for the $M2$ transition, the isomeric decay from the 204.8-keV (3^+) level of ^{106}Nb, and similar changes in triaxial deformation of the bandheads compared to those in the ground levels also were calculated in ^{104,106}Nb.

It is interesting to note that, in ^{104,106}Nb, none of the configurations have a minimum energy near maximum triaxiality of 30°, but rather show minima near 15°. This feature may be a characteristic of the high-j proton and neutrons just beginning to fill, whereas, the half-filled shells would favor near-maximum triaxiality.

C. The energy levels, moments of inertia $J^{(1)}$ versus $\hbar\omega$, and $E(I) - E(I-1)$ versus spin of the rotational band observed in ^{104,106}Nb

The PSM calculations that reproduced level energies, moments of inertia $J^{(1)}$, and $E(I) - E(I-1)$ of the bands in ^{104,106}Nb provided further evidence for the assignments to the bands. The best comparisons between the PSM and the experimental data for the chosen theoretical configurations are given in Figs. 8–13. The spin-parity $K^\pi = 2^-$ and

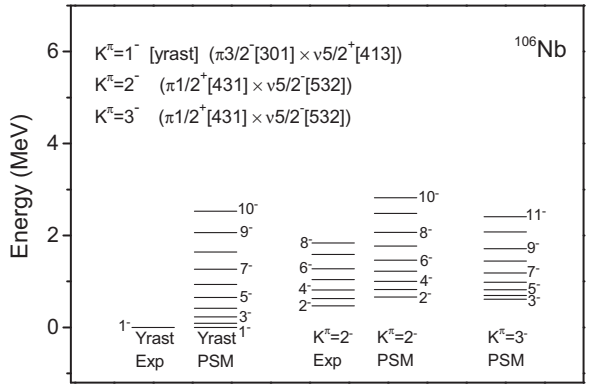

FIG. 8. Calculated energy levels for the band in ^{106}Nb by PSM based on $K^\pi = 2^-$, $\pi 1/2^+[431] \times \nu 5/2^-[532]$, $K^\pi = 3^-$, $\pi 1/2^+[431] \times \nu 5/2^-[532]$, and comparison with the data. The yrast band built on the ground level with $K^\pi = 1^-$, yrast $\pi 3/2^-[301] \times \nu 5/2^+[413]$ also was calculated. The best match for the band observed in ^{106}Nb was achieved by the PSM calculations with the assignment of $K^\pi = 2^-$ to the bandhead.

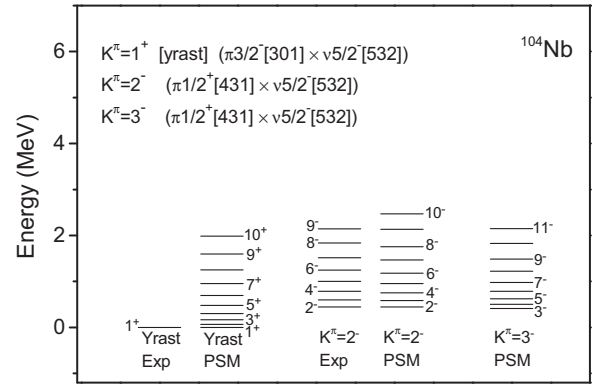

FIG. 9. Calculated energy levels for the band in ^{104}Nb by PSM based on $K^\pi = 2^-$, $\pi 1/2^+[431] \times \nu 5/2^-[532]$, $K^\pi = 3^-$, $\pi 1/2^+[431] \times \nu 5/2^-[532]$, and comparison with the data. The yrast band built on the ground level with $K^\pi = 1^+$, yrast $\pi 3/2^-[301] \times \nu 5/2^-[532]$ also was calculated. The best match for the band observed in ^{104}Nb was achieved by the PSM calculations with the assignment of $K^\pi = 2^-$ to the bandhead.

configuration $\pi 1/2^+[431] \times \nu 5/2^-[532]$ well reproduce all the $E_{\rm exc}$ of the levels, moments of inertia $J^{(1)}$ versus $\hbar\omega$, and $E(I) - E(I-1)$ versus spin for the bands in ^{104,106}Nb, which is in good agreement with the assignments to the bandheads by the PES calculations discussed above. It is worth mentioning that obvious disagreements were seen between the experimental data of ^{106}Nb and the PSM calculations based on the four configurations with excitations lower than that of $\pi 1/2^+[431] \times \nu 5/2^-[532]$ as listed in the fifth through eighth row, respectively, in Table II.

Figure 8 indicates the calculated energy levels of ^{106}Nb for $K^\pi = 1^-$, yrast $\pi 3/2^-[301] \times \nu 5/2^+[413]$; $K^\pi = 2^-$, $\pi 1/2^+[431] \times \nu 5/2^-[532]$, and $K^\pi = 3^-$, $\pi 1/2^+[431] \times \nu 5/2^-[532]$, respectively, and makes a comparison with the experimental data. As can be seen in Fig. 8, the observed band built on the bandhead, the 470.6-keV level in ^{106}Nb, was best reproduced by $K^\pi = 2^-$, $\pi 1/2^+[431] \times \nu 5/2^-[532]$, the same as assigned to the bandhead by the PES calculations (see Table II). Although no experimental yrast band built on the ground level was observed and was compared with the theoretical $K^\pi = 1^-$, yrast $\pi 3/2^-[301] \times \nu 5/2^+[413]$ band, the assignment of $K^\pi = 1^-$, $\pi 3/2^-[301] \times \nu 5/2^+[413]$ to the ground level is consistent with that given by the PES calculations. The same is shown in Fig. 9 for ^{104}Nb, but the theoretical level spacing and level pattern, instead of level energies, are compared with the experimental data since the experimental excitation of the bandhead was not determined in ^{104}Nb. In Fig. 9, it can be seen that the best fit for the band built on the bandhead, the $(130.5 + x)$-keV level observed in ^{104}Nb, is achieved by calculations based on $K^\pi = 2^-$, $\pi 1/2^+[431] \times \nu 5/2^-[532]$, the same as given by the PES calculations (see Table III), and the same as assigned to the analogous band in ^{106}Nb (see Fig. 8 and Tables II and III). In Fig. 9, the theoretical $K^\pi = 1^+$, yrast $\pi 3/2^-[301] \times \nu 5/2^-[532]$ band also was calculated for ^{104}Nb, which may have provided additional evidence that, most unlikely, the 130.5-keV transition directly feeds the ground level. The predicted $K^\pi = 1^+$ band built on the ground level has considerably different level spacings and level patterns in comparison with those of the band observed.

Shown in Figs. 10 and 11 are the theoretical moments of inertia $J^{(1)}$ versus $\hbar\omega$ for the bands in ^{106}Nb and ^{104}Nb, respectively, in comparison with the experimental data. Calculations for $K^\pi = 2^-$ and $K^\pi = 3^-$ with configuration $\pi 1/2^+[431] \times \nu 5/2^-[532]$ are shown in (a) and (b) of the two figures, respectively. In Figs. 10 and 11, one can see that only the fit with $K^\pi = 2^-$, $\pi 1/2^+[431] \times \nu 5/2^-[532]$ can reproduce the experimental $J^{(1)}$ well. Very large disagreement between theory and experiment is seen for calculations with $K^\pi = 3^-$, $\pi 1/2^+[431] \times \nu 5/2^-[532]$, so assignments of $K^\pi = 3^-$ to the bandheads are definitely excluded. The theoretical $E(I) - E(I-1)$ versus spin curves based on

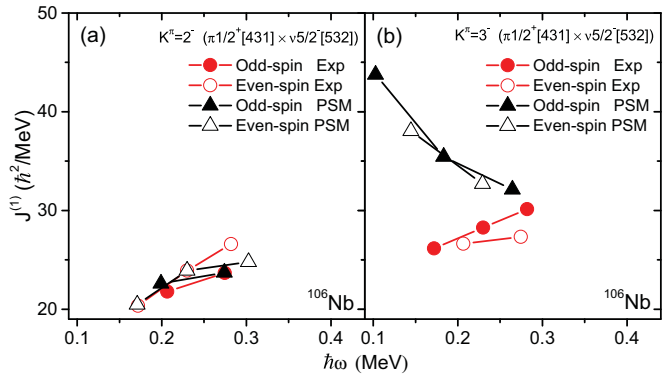

FIG. 10. (Color online) The theoretical moments of inertia $J^{(1)}$ versus $\hbar\omega$ calculated for ^{106}Nb by PSM based on (a) $K^\pi = 2^-$, $\pi 1/2^+[431] \times \nu 5/2^-[532]$ and (b) $K^\pi = 3^-$, $\pi 1/2^+[431] \times \nu 5/2^-[532]$ in comparison with the data. It is necessary to emphasize that the same experimental data are plotted in (a) and (b), just with different assumed bandhead spins. Although $J^{(1)}$ versus $\hbar\omega$ of the band observed in ^{106}Nb was well reproduced by the PSM calculations with $K^\pi = 2^-$, very large disagreement is seen for the assignment of $K^\pi = 3^-$.

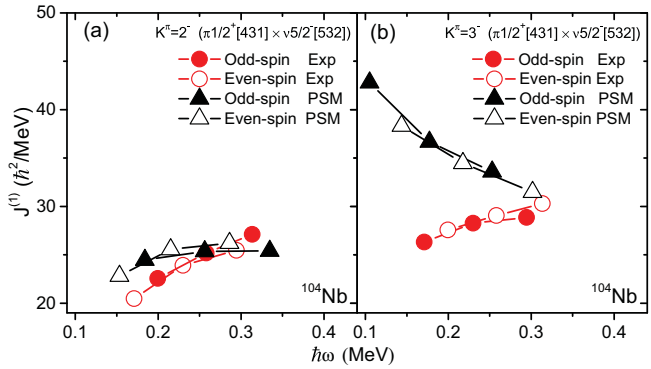

FIG. 11. (Color online) The theoretical moments of inertia $J^{(1)}$ versus $\hbar\omega$ calculated for ^{104}Nb by PSM based on (a) $K^\pi = 2^-$, $\pi 1/2^+[431] \times \nu 5/2^-[532]$ and (b) $K^\pi = 3^-$, $\pi 1/2^+[431] \times \nu 5/2^-[532]$ in comparison with the data. It is necessary to emphasize that the same experimental data are plotted in (a) and (b), just with different assumed bandhead spins. Although $J^{(1)}$ versus $\hbar\omega$ of the band observed in ^{104}Nb was well reproduced by the PSM calculations with $K^\pi = 2^-$, very large disagreement is seen for the assignment of $K^\pi = 3^-$.

the configuration $\pi 1/2^+[431] \times \nu 5/2^-[532]$, $K^\pi = 2^-$ and $K^\pi = 3^-$ are compared to the experimental data in Figs. 12 and 13 for the bands of ^{106}Nb and ^{104}Nb, respectively. Calculations for $K^\pi = 2^-$ and $K^\pi = 3^-$ with configuration $\pi 1/2^+[431] \times \nu 5/2^-[532]$ are shown in (a) and (b) of the two figures, respectively. Again, one can see that, with the same configuration $\pi 1/2^+[431] \times \nu 5/2^-[532]$, good matching is achieved for the $K^\pi = 2^-$ assignment to the bandheads of ^{104,106}Nb, and considerable discrepancies of theoretical $E(I) - E(I-1)$ versus spin from the experimental data are seen for a $K^\pi = 3^-$ assignment to the bandheads. The very good agreements between theory and experiment shown in Figs. 8–13 strongly support the assignments of configuration and spin-parity $\pi 1/2^+[431] \times \nu 5/2^-[532]$, $K^\pi = 2^-$ to the bandheads of ^{106}Nb and ^{104}Nb.

The PES and PSM calculations provided valuable information that concerned configurations, spin-parity, shapes, and interpretations for the decay properties of the bands of ^{104,106}Nb and confirmed the spin-parity assignments as indicated in Figs. 3 and 4. It should be noted that reassignments of spin-parity were performed in the present paper for the level scheme of ^{104}Nb (Fig. 4). In Ref. [8], even parity was tentatively assigned to the band, and (3^+) was assigned to the bandhead in ^{104}Nb. As mentioned above, the lack of ground feeding from the $(130.5 + x)$-keV level and its very weak 130.5-keV decaying transition in ^{104}Nb can be explained by a long enough half-life that prevents experimental observations for them in various studies to date; the latter may also be due to the changes in both proton and neutron orbitals in the initial and final states. The $M2$ character can be a further reason for the missing of the ground feeding from the very weakly populated x-keV (3^-) level of ^{104}Nb.

Shown in Fig. 14 is the experimental $E(I) - E(I-1)$ versus spin and in Fig. 15, the moments of inertia $J^{(1)}$ versus $\hbar\omega$, respectively, for the analogous bands in ^{102,104,106}Nb. An overall similarity is seen in Figs. 14 and 15 from low to medium spins, which supports not only the establishment of level schemes, but also the configuration and spin-parity assignments by PES and PSM model calculations. The level systematics and similarities shown in Figs. 14 and 15 support the assignments based on PES and PSM calculations for ^{104,106}Nb, and it can, thus, be understood that the same configuration and spin-parity were assigned to the band in ^{104,106}Nb by both PES and PSM calculations. However, at higher spin-rotational frequency regions, one can see irregularities and discrepancies that occur in the bands of ^{104,106}Nb (Figs. 14 and 15). And one can see differences in $J^{(1)}$ that develop with changing neutron numbers in Fig. 15. Although the bands are not extended high enough to reveal band crossings, we hoped to make total Routhian surface (TRS) calculations to study the band evolution with increasing rotational frequencies, but, however, since the intruder orbital was found to be involved in the bandheads of the Nb isotopes, the TRS calculation with the available code would not be convergent.

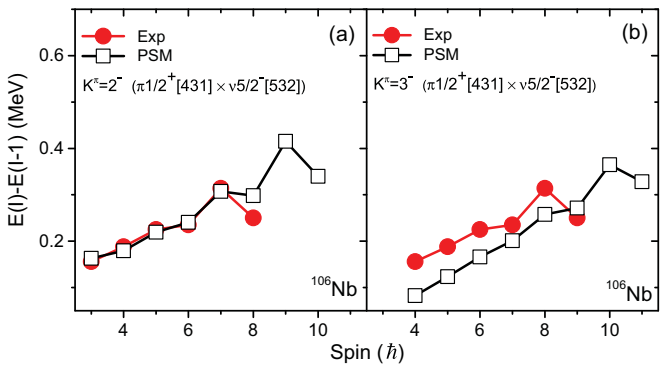

FIG. 12. (Color online) Theoretical $E(I) - E(I-1)$ versus spin curves calculated for ^{106}Nb by PSM based on (a) $K^\pi = 2^-$, $\pi 1/2^+[431] \times \nu 5/2^-[532]$ and (b) $K^\pi = 3^-$, $\pi 1/2^+[431] \times \nu 5/2^-[532]$ in comparison with the data. It is necessary to emphasize that the same experimental data are plotted in (a) and (b), just with different assumed bandhead spins. Again, good matching is seen for the assignment of $K^\pi = 2^-$ to the bandhead of ^{106}Nb.

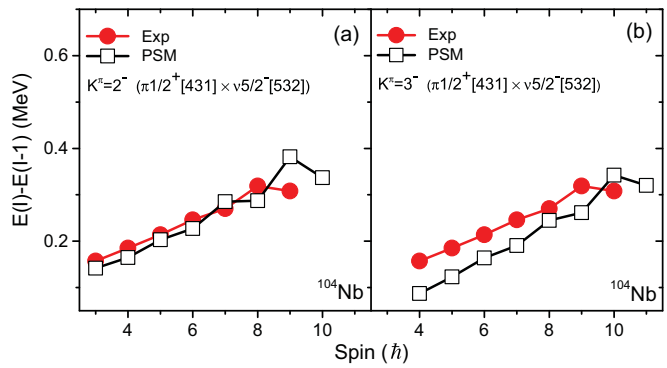

FIG. 13. (Color online) Theoretical $E(I) - E(I-1)$ versus spin curves calculated for ^{104}Nb by PSM based on (a) $K^\pi = 2^-$, $\pi 1/2^+[431] \times \nu 5/2^-[532]$ and (b) $K^\pi = 3^-$, $\pi 1/2^+[431] \times \nu 5/2^-[532]$ in comparison with the data. It is necessary to emphasize that the same experimental data are plotted in (a) and (b), just with different assumed bandhead spins. Again, good matching is seen for the assignment of $K^\pi = 2^-$ to the bandhead of ^{104}Nb.

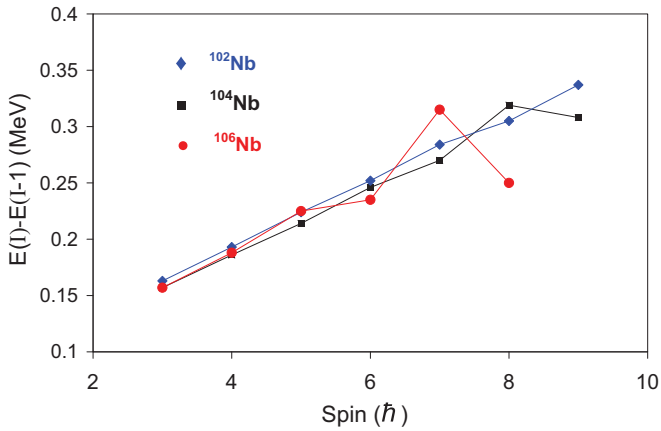

FIG. 14. (Color online) Experimental $E(I) - E(I-1)$ versus spin of the analogous bands in ^{102,104,106}Nb. An overall similarity in low to medium spins can be seen in ^{102,104,106}Nb. See the text for discussions.

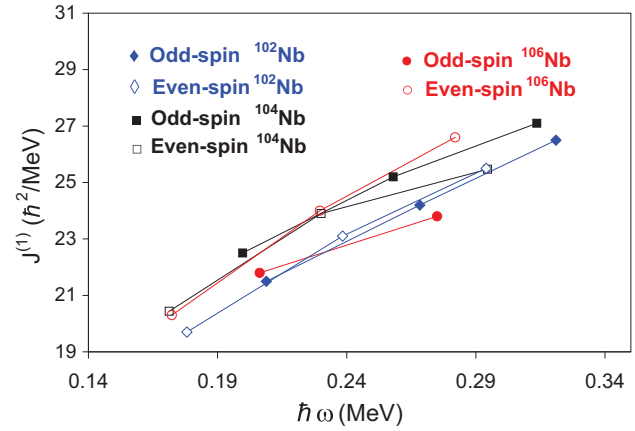

FIG. 15. (Color online) Experimental $J^{(1)}$ plotted against rotational frequencies $\hbar\omega$ for the analogous bands in ^{102,104,106}Nb. Similar $J^{(1)}$ and evolving differences with changing neutron numbers can be seen in the figure. See the text for discussions.

Very recently, based on our 4D hypercube data and PES and triaxial projected shell model calculations, Li *et al.* [30] reinvestigated the level scheme of ^{105}Nb, the neighboring odd-even isotopes of ^{104,106}Nb. The previously reported yrast band [5] was confirmed and was assigned as $K^\pi = 5/2^+$, $\pi 5/2^+[422]$, $\gamma = 12.3°$, $\beta_2 = 0.339$, $\beta_4 = 0.007$. This proton orbital probably couples with the odd neutron to form higher-energy bands (see Tables II and III) above those shown in our level schemes, and these bands are too weakly populated to observe in our odd-odd studies.

IV. SUMMARY

The first observation of a rotational band in very neutron-rich ^{106}Nb and the extension of a similar band previously reported in ^{104}Nb were achieved by means of γ-γ-γ and γ-γ-γ-γ measurements of prompt fission γ rays from ^{252}Cf. Based on our high-statistics data, the identification of the band in ^{106}Nb was made by the coincidence of the band with fission partners and the previously reported low-lying transitions, which were observed in both double- and triple-gated spectra in the present paper. The measurements of fission yield ratios between ^{106}Nb and ^{104}Nb in double-gated spectra with changing gates set in their different fission partners provided additional evidence for the band assignment. PES and PSM calculations have successfully reproduced the newly proposed level scheme of ^{106}Nb and the extended one of ^{104}Nb. For these nuclei with large quadrupole deformations, the occupation of the proton intruder orbital $\pi 1/2^+[431]$ helps to explain the isomeric decay and reveals a shape evolution from partially triaxial deformation at ground level to nearly axially symmetric shapes in isomeric states and bandheads of both Nb isotopes. Good fits for the rotational bands observed in ^{104,106}Nb were achieved by PSM calculations based on $K^\pi = 2^-$, $\pi 1/2^+[431] \times \nu 5/2^-[532]$, which are consistent with the assignments to the bandheads by the PES calculations, which again show the role played by the proton intruder orbital $\pi 1/2^+[431]$. A puzzle remains in ^{106}Nb, that is why the 337.6-keV (2^-) level decays by $E1$ to the 204.8-keV (3^+) level but not by $E1$ to the 202.2-keV (2^+) level. Further experimental and theoretical studies are needed to shed light upon the 204.8- and 202.2-keV levels with so similar excitations and half-lives. Further experimental and theoretical studies may also be needed for the decay out of the bandhead of ^{104}Nb.

ACKNOWLEDGMENTS

The work at Vanderbilt University, Lawrence Berkeley National Laboratory, Lawrence Livermore National Laboratory, Mississippi State University, and Idaho National Laboratory was supported by the U.S. DOE Grants No. DE-FG-05-88ER40407, No. DE-FG02-95ER40934, No. DE-AC52-07NA27344, No. DE-FG02-95ER40939, and No. DE-AC07-761DO1570 and Contract No. W-7405-ENG48. The work at SJTU in Shanghai was supported by the NNSF of China under Grants No. 11135005 and No. 11075103 and by the 973 Program of China (Grant No. 2013CB834401). The work at Tsinghua University in Beijing was supported by the NNSF of China Grant No. 11175095 and the Special Program of HESF Grant No. 20100002110077. The work at HUTC in Huzhou was supported by the NNSF of China Grants No. 11305059, No. 11275067, and No. 11275068.

[1] J. Skalski, S. Mizutori, and W. Nazarewicz, Nucl. Phys. A **617**, 282 (1997).
[2] J. H. Hamilton, Prog. Part. Nucl. Phys. **15**, 107 (1985); *Treatise on Heavy Ion Science*, edited by D. A. Bromley, Vol. 8 (Plenum, New York, 1989), p. 2 and references therein.
[3] Y. X. Luo *et al.*, Phys. Rev. C **69**, 024315 (2004).
[4] Y. X. Luo, J. O. Rasmussen, J. H. Hamilton, A. V. Ramayya, J. K. Hwang, S. J. Zhu, P. M. Gore, S. C. Wu, I. Y. Lee, P. Fallon, T. N. Ginter, G. M. Ter-Akopian, A. V. Daniel, M. A. Stoyer, R. Donangelo, and A. Gelberg, Phys. Rev. C **70**, 044310 (2004).

[5] Y. X. Luo *et al.*, J. Phys. G: Nucl. Part. Phys. **31**, 1303 (2005).
[6] J. K. Hwang *et al.*, Phys. Rev. C **58**, 3252 (1998).
[7] J. K. Hwang *et al.*, J. Phys. G: Nucl. Part. Phys. **27**, L9 (2001).
[8] J. G. Wang *et al.*, Phys. Rev. C **78**, 014313 (2008); Chinese Phys. C **33**, 158 (2009).
[9] J. G. Wang *et al.*, Phys. Lett. B **675**, 420 (2009).
[10] Y. X. Luo *et al.*, Nucl. Phys. A **825**, 1 (2009).
[11] K. Shizuma *et al.*, Z. Phys. A **311**, 71 (1983).
[12] J. Pereira *et al.*, Phys. Rev. C **79**, 035806 (2009).
[13] J. Genevey, F. Ibrahim, J. A. Pinston, H. Faust, T. Friedrichs, M. Gross, and S. Oberstedt, Phys. Rev. C **59**, 82 (1999).
[14] D. Kameda *et al.*, Phys. Rev. C **86**, 054319 (2012).
[15] J. H. Hamilton *et al.*, Prog. Part. Nucl. Phys. **35**, 635 (1995).
[16] D. C. Radford, Nucl. Instrum. Methods Phys. Res., Sect. A **361**, 297 (1995), also cf. his website http://radware.phy.ornl.gov/
[17] Y. X. Luo *et al.* (to be published).
[18] J. H. Hamilton *et al.*, Phys. Rep. **264**, 215 (1996); S.-C. Wu, R. Donangelo, J. O. Rasmussen, A. V. Daniel, J. K. Hwang, A. V. Ramayya, and J. H. Hamilton, Phys. Rev. C **62**, 041601(R) (2000).
[19] K. Hara and Y. Sun, Int. J. Mod. Phys. E **4**, 637 (1995).
[20] Y. Sun and K. Hara, Comput. Phys. Commun. **104**, 245 (1997).
[21] P. Möller *et al.*, At. Data Nucl. Data Tables **59**, 185 (1995).
[22] Y.-X. Liu *et al.*, Nucl. Phys. A **858**, 11 (2011).
[23] F. R. Xu, P. M. Walker, J. A. Sheikh, and R. Wyss, Phys. Lett. B **435**, 257 (1998).
[24] F. R. Xu, P. M. Walker, and R. Wyss, Phys. Rev. C **65**, 021303(R) (2002).
[25] W. Nazarewicz, J. Dudek, R. Bengtsson, T. Bengtsson, and I. Ragnarsson, Nucl. Phys. A **435**, 397 (1985).
[26] H. C. Pradhan, Y. Nogami, and J. Law, Nucl. Phys. A **201**, 357 (1973).
[27] P. Möller and J. R. Nix, Nucl. Phys. A **536**, 20 (1992).
[28] W. D. Myers and W. J. Swiatecki, Nucl. Phys. **81**, 1 (1966).
[29] V. M. Strutinsky, Nucl. Phys. A **95**, 420 (1967).
[30] H. J. Li *et al.*, Phys. Rev. C **88**, 054311 (2013).